Orai3 TM3 point mutation G158C alters kinetics of 2-APB–induced gating by disulfide bridge formation with TM2 C101

Anna Amcheslavsky, Olga Safrina, and Michael D. Cahalan

Department of Physiology and Biophysics, University of California, Irvine, Irvine, CA 92697

After endoplasmic reticulum (ER) Ca^{2+} store depletion, Orai channels in the plasma membrane (PM) are activated directly by ER-resident STIM proteins to form the Ca^{2+}-selective Ca^{2+} release–activated Ca^{2+} (CRAC) channel. However, in the absence of Ca^{2+} store depletion and STIM interaction, the mammalian homologue Orai3 can be activated by 2-aminoethyl diphenylborinate (2-APB), resulting in a nonselective cation conductance characterized by biphasic inward and outward rectification. Here, we use site-directed mutagenesis and patch-clamp analysis to better understand the mechanism by which 2-APB activates Orai3. We find that point mutation of glycine 158 in the third transmembrane (TM) segment to cysteine, but not alanine, slows the kinetics of 2-APB activation and prevents complete channel closure upon 2-APB washout. The "slow" phenotype exhibited by Orai3 mutant G158C reveals distinct open states, characterized by variable reversal potentials. The slow phenotype can be reversed by application of the reducing reagent bis(2-mercaptoethylsulfone) (BMS), but in a state-dependent manner, only during 2-APB activation. Moreover, the double mutant C101G/G158C, in which an endogenous TM2 cysteine is changed to glycine, does not exhibit altered kinetics of 2-APB activation. We suggest that a disulfide bridge, formed between the introduced cysteine at TM3 position 158 and the endogenous cysteine at TM2 position 101, hinders transitions between Orai3 open and closed states. Our data provide functional confirmation of the proximity of these two residues and suggest a location within the Orai3 protein that is sensitive to the actions of 2-APB.

The Journal of General Physiology

INTRODUCTION

Store-operated calcium entry (SOCE) enables calcium ions (Ca^{2+}) to enter cells in response to depletion of ER Ca^{2+} stores, raising cytosolic Ca^{2+} levels, refilling Ca^{2+} stores, and ultimately turning on signaling cascades responsible for secretion, gene transcription, alterations in motility, and cell proliferation (Putney, 1986; Bootman et al., 2001; Parekh and Putney, 2005; Cahalan, 2009). A series of RNAi screens led to the molecular identification of two key proteins, STIM and Orai, that underlie SOCE in numerous cell types (Liou et al., 2005; Roos et al., 2005; Zhang et al., 2005; Feske et al., 2006; Vig et al., 2006a). There are two mammalian homologues of STIM, STIM1 and STIM2, and three of Orai, Orai1, Orai2, and Orai3. Together, STIM1 and Orai1 form the highly Ca^{2+}-selective Ca^{2+} release–activated Ca^{2+} (CRAC) channel of T lymphocytes. ER membrane–resident STIM proteins are Ca^{2+} sensors capable of detecting Ca^{2+} store depletion (Liou et al., 2005; Zhang et al., 2005). Plasma membrane (PM)–bound Orai proteins are the pore-forming subunits of the CRAC channel (Prakriya et al., 2006; Vig et al., 2006b; Yeromin et al., 2006). Upon ER Ca^{2+} store depletion, STIM molecules translocate to cortical ER–PM junctions, where they physically interact with and activate Orai (Cahalan, 2009; Soboloff et al., 2012).

Apart from opening in response to ER Ca^{2+} store depletion via STIM1 interaction, Orai3 can be activated in a STIM1-independent manner by 2-aminoethyl diphenylborinate (2-APB; Lis et al., 2007; DeHaven et al., 2008; Peinelt et al., 2008; Zhang et al., 2008). 2-APB activates Orai3 channels by opening and dilating the conducting pore (Schindl et al., 2008), resulting in a nonselective, inwardly and outwardly rectifying cationic current. By using Orai1 and Orai3 chimeras, we have previously shown that the TM2-TM3 region of Orai3 is necessary for activation by 2-APB (Zhang et al., 2008). Furthermore, mutation G183A in TM3 of Orai1 results in Orai1 channels that respond to 2-APB in a fashion similar to Orai3 channels (Srikanth et al., 2011).

Here, we use cysteine and alanine substitution along with electrophysiological techniques to probe the conserved Orai3 glycine residue at the middle of TM3, G158, to understand what part this structural "hinge" may play in 2-APB activation. Our evidence points to close proximity of particular residues in TM3 and TM2, as indicated by functional effects of disulfide bond–reducing reagent bis(2-mercaptoethylsulfone) (BMS). We propose that TM3 position 158 mutated to a cysteine residue can interact with the endogenous TM2 C101 to form a disulfide bridge that can only be reduced by BMS during

Correspondence to Michael D. Cahalan: mcahalan@uci.edu

Abbreviations used in this paper: 2-APB, 2-aminoethyl diphenylborinate; BMS, bis(2-mercaptoethylsulfone); CRAC, Ca^{2+} release–activated Ca^{2+}; PM, plasma membrane.

The Rockefeller University Press $30.00
J. Gen. Physiol. Vol. 142 No. 4 405–412
www.jgp.org/cgi/doi/10.1085/jgp.201311030

2-APB activation. Moreover, this disulfide bridge hinders 2-APB in its mechanism of activation, thereby altering the kinetics of 2-APB–induced channel activation and deactivation. We discuss these results in the context of a recently published crystal structure of *Drosophila melanogaster* Orai (Hou et al., 2012).

MATERIALS AND METHODS

Molecular biology

A previously described construct, EGFP-Orai3-WT (Demuro et al., 2011), was used as both WT control and as the template for the generation of mutant cDNA. In brief, a 5′ EcoR1 digestion site was added to the N-terminal cDNA sequence of the *Orai3* gene (omitting the first ATG codon), and a 3′ BamHI digestion site was added to the C-terminal cDNA sequence of the *Orai3* gene (after the STOP codon). This *Orai3* gene was then subcloned by EcoR1–BamH1 (New England Biolabs, Inc.) to pEGFP-C2 (Takara Bio Inc.), resulting in the construct EGFP-Orai3-WT. We used the QuikChange Lightning Site-Directed Mutagenesis kit (Agilent Technologies) to generate Orai3 mutants. All PCR products were subcloned to new pEGFP-C2 backbone after mutagenesis by EcoR1–BamH1. EGFP-Orai3-G158C and EGFP-Orai3-G158A were made on template EGFP-Orai3-WT. All double mutants were made on template EGFP-Orai3-G158C. Maxipreps of all constructs were prepared with QIAfilter Plasmid Maxi kit (QIAGEN) and sequenced by Eton Biosciences. All constructs used in this study are EGFP tagged at the N terminus to facilitate visual identification of transfected cells. For simplicity, "EGFP" is omitted from construct names throughout the text.

Primers used are as follows: G158C forward, 5′-CTTCTCCACTGCCCTGTGCACCTTTCTCTTCC-3′; and reverse, 5′-GGAAGAGAAAGGTGCACAGGGCAGTGGAGAAG-3′; G158A forward, 5′-CTCCACTGCCCTGGCCACCTTTCTCTTCC-3′; and reverse, 5′-GGAAGAGAAAGGTGGCCAGGGCAGTGGAG-3′; C101G forward, 5′-GCCTTCAGTGCCGGCACCACCGTGC-3′; and reverse, 5′-GCACGGTGGTGCCGGCACTGAAGGC-3′; and sequencing forward, 5′-CATGGTCCTGCTGGAGTTCGTG-3′; and reverse, 5′-CCTCTACAAATGTGGTATGG-3′.

Cell culture

Human embryonic kidney (HEK) 293A cells (Invitrogen) were incubated at 37°C, 5% CO_2, and maintained in Dulbecco's modified Eagle's medium (DMEM; Lonza) supplemented with 10% fetal calf serum (Omega Scientific) and 2 mM L-glutamine (Sigma-Aldrich). Cells were passed twice per week. With each passage, cells were rinsed with 2 mM EDTA-PBS solution, trypsinized (Sigma-Aldrich), diluted 1:10 in fresh DMEM, and then transferred to new sterile T75 Corning flasks. For experiments, cells were plated onto 6-well plate dishes and given 24–72 h to grow to ∼95% confluency for transfection by Lipofectamine 2000 (Invitrogen), as advised by Invitrogen, with 1× OPTI-MEM I (Gibco).

Electrophysiology

HEK 293A cells were lifted 24 h after transfection, plated onto custom chambers coated with 100 µg/ml of sterile poly-lysine (Sigma-Aldrich), and kept at 37°C overnight. Cells were chosen for whole-cell recording by expression of EGFP, 24 h after replating.

Pipettes were pulled, Sylgarded, and fire-polished to ∼2 MΩ resistance. Patch-clamp experiments were performed at room temperature in standard whole-cell recording. Only cells with high input resistance (>1 GΩ) were selected for recording. The series resistance (2–7 MΩ) was compensated by 80%. Membrane potentials were corrected for the liquid junction potential of 10 mV between the pipette and bath solution. Currents were recorded using an EPC-9 patch-clamp amplifier (HEKA). Protocols were generated and data acquired by PULSE (HEKA). Data were digitally filtered at 1 kHz for analysis and display. Our general protocol alternated voltage ramps lasting 220 ms from −120 to 100 mV and pulses of 220 ms to −120 mV every 2 s from a holding potential of 0 mV. Five I-V curves were averaged for display. Leak currents before channel activation were averaged (five sweeps) and subtracted from subsequent current records. Unless otherwise stated, leak-subtracted I-V curves are displayed. Whole-cell current amplitudes were normalized to measured cell capacitance values to obtain current densities (pA/pF). Data were analyzed and graphed in OriginPro 7.5.

The external solution consisted of (mM) 151.5 NaCl, 4.5 KCl, 2 $CaCl_2$, 10 HEPES, and 10 glucose, pH adjusted to 7.4 by NaOH, osmolality adjusted to 325 mOsm/kg by sucrose. This external solution was used as a standard for all others. 2-APB was added from 100-mM stock (2-APB powder [Sigma-Aldrich] dissolved in DMSO). BMS (EMD Millipore) was freshly prepared the day of the experiment, added to warmed external solution, and vortexed to assist in solubilization. The internal solution consisted of (mM) 144 CsAsp, 8 Mg-gluconate$_2$, 2 CsCl, 15 HEPES, 12 Cs_4EGTA, and 2.5 $Ca(OH)_2$, pH adjusted to 7.2 by CsOH, with a free [Ca^{2+}] of 50 nM (calculated by Maxchelator) and osmolality of 330 mOsm/kg.

Online supplemental material

Fig. S1 shows partial, reversible, BMS-induced block of 2-APB–activated current carried by Orai3-WT channels. Fig. S2 shows that a higher concentration (1 mM) of 2-APB does not increase the rate of 2-APB activation of Orai3-G158C; instead, 1 mM 2-APB partially blocks currents carried by both Orai3-WT and Orai3-G158C. Fig. S3 shows gradual leftward shift of I-V relationships produced by 2-APB–activated Orai3-G158C channels; I-V relationships were taken every 1 min after 2-APB application for 5 min. Fig. S4 shows a bar graph summarizing total 2-APB–activated current amplitudes of three Orai3 double mutants: Orai3-C101G/G158C, Orai3-C101A/G158C, and Orai3-C101S/G158C. Online supplemental material is available at http://www.jgp.org/cgi/content/full/jgp.201311030/DC1.

RESULTS

Mutation G158C alters kinetics of 2-APB activation and washout

Upon extracellular application of 100 µM 2-APB, cells transfected with Orai3-WT exhibited inwardly and outwardly rectifying currents that activated rapidly and exponentially until saturation ($n = 4$). Compared with Orai3-WT channels, Orai3-G158C channels activated at a much slower rate and did not saturate ($n = 4$). In contrast, Orai3-G158A channels, with nonreactive alanine residues as opposed to the cysteine residues of Orai3-G158C that may form disulfide bridges, mimicked Orai3-WT channels, activating rapidly and reaching saturation ($n = 5$). Data are summarized by the time courses in Fig. 1 (A and B). Overall, Orai3-G158C channels exhibited an eightfold decrease in the initial rate of rise of 2-APB–activated current (Fig. 1 I).

I-V shapes produced by mutants Orai3-G158C (Fig. 1, D and G) and Orai3-G158A (Fig. 1, E and H) were similar to those of Orai3-WT (Fig. 1, C and F) channels;

both sets of mutant channels still carried a nonselective, inwardly and outwardly rectifying current. However, as a result of the perturbed, slow response to 2-APB activation, current densities carried by Orai3-G158C channels were reduced and failed to saturate within 5 min. 5 min after addition of 2-APB, both Orai3-WT and Orai3-G158A channels exhibited currents with amplitudes approximately three times greater than those of Orai3-G158C channels (Fig. 1 J).

After 2-APB washout, Orai3-WT channels closed within 2 min as current densities rapidly and exponentially fell to zero (Fig. 1, B and F). However, Orai3-G158C channels failed to close (deactivate) after 2-APB washout, resulting in a residual current of 15.8 ± 3.2% and 6.4 ± 1.0% of the maximal inward and outward currents, respectively, recorded during the preceding 2-APB treatment (Fig. 1, B and G). Orai3-G158A channels recovered from 2-APB treatment with rates not significantly different from Orai3-WT, and they closed completely (Fig. 1, B and H). These data are summarized by bar graphs in Fig. 1 K. Collectively, these results indicate that the G158C mutation results in a slow 2-APB–gating phenotype, and the G158A mutation indicates that this is probably not solely caused by decreased conformational flexibility within TM3.

G158C suggests multiple open 2-APB–activated states

Because Orai3-G158C channels continued to conduct upon 2-APB washout, we sought to understand how the mutation might affect channel function during consecutive applications and washouts of 2-APB (Fig. 2, A and B). We applied 100 µM 2-APB during whole-cell recordings for 2-min intervals, separated by 1-min-long washout periods, and found that with each reapplication of 2-APB, current densities jumped to amplitudes similar to those before 2-APB washout (Fig. 2 A). This result suggests that after 2-APB washout, mutant channels remain in a state that is easier to activate than the closed channel state. Furthermore, current density remaining after 2-APB washout increased in amplitude with each subsequent sequence of 2-APB application/washout (Fig. 2 B). Perhaps most interestingly, the reversal potentials of currents carried during consecutive 2-APB applications gradually shifted leftward (Fig. 2, A, C, and E). Moreover, after these 2-APB

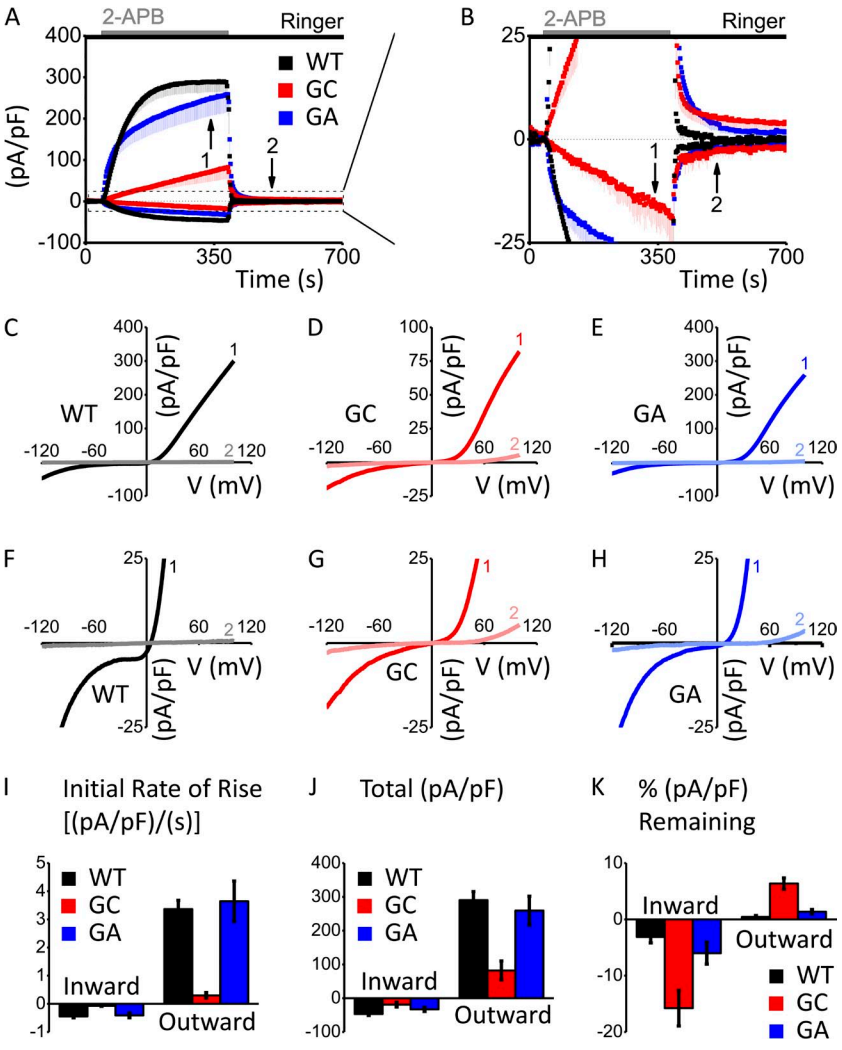

Figure 1. Mutation G158C alters the kinetics of 2-APB activation and washout. Whole-cell currents were normalized to whole-cell capacitance to yield current densities. (A and B) Time course of Orai3-WT (WT; n = 4), Orai3-G158C (GC; n = 4), and Orai3-G158A (GA; n = 5), activated by 100 µM 2-APB, represented as mean current density ± SEM (pA/pF) versus time (s). For clarity, only minus SEM is shown. (C–E) I-V relationships corresponding to current density 5 min after 2-APB application (1) and 2 min after 2-APB washout (2) for WT, GC, and GA, respectively. (F–H) Same I-V relationships as in C–E, but zoomed in to emphasize the large fraction of current remaining after 2-APB washout for the Orai3-G158C mutant (G). (I) Rates of rise of inward and outward components of the 2-APB–activated current densities (pA/pF)/s during the first 30 s of recording after initial 2-APB application for WT, GC, and GA. (J) Current densities (pA/pF) 5 min after 2-APB application for WT, GC, and GA. (K) Percent current density remaining 2 min after 2-APB washout, normalized to maximal current density recorded 5 min after 2-APB application. Error bars show SEM.

applications, the I-V relationships of residual currents exhibited progressively decreasing reversal potentials (Fig. 2, B, D, and F). This leftward shift of reversal potentials has been observed previously for WT Orai3 channels (Schindl et al., 2008). Here, we suggest that the G158C mutant is trapped in several distinct open states during 2-APB treatment, resulting in reversal potentials that range from 46.5 to 6.5 mV. We suggest that the mechanism by which 2-APB activates Orai3 involves a series of conformational changes, which result in several distinct open states, each characterized by the extent of pore dilation and a correspondingly decreased reversal potential.

State-dependent reversal of G158C "slow" phenotype by BMS application during 2-APB activation

Because the G158C mutation, but not G158A, alters the kinetics of 2-APB activation and washout, we sought to understand whether the introduced cysteine forms a disulfide bridge with another cysteine in the vicinity. If that were the case, then reducing the hypothesized disulfide bridge would revert the slow G158C phenotype back to WT-like kinetics. To test this hypothesis, we used the reducing reagent BMS before or during the slow activation of Orai3-G158C by 2-APB. For comparison, without BMS treatment, 2-APB application caused a slow, linear rise in inward and outward currents (Fig. 3, A and D; see also Figs. 1 and 2). When BMS was added to standard external solution and then removed before 2-APB application, 2-APB–activated currents were not greatly altered (Fig. 3, B and E). In contrast, BMS treatment during 2-APB application resulted in Orai3-G158C currents that rose rapidly and exponentially, similar to Orai3-WT. Furthermore, the reversal potential quickly shifted leftward to ∼2.5 mV (Fig. 3, C, F, and G), thus mimicking the kinetics, rectification, and shift in reversal potential of Orai3-WT channels without BMS treatment (as shown in Fig. 1 A, C, and F; and Fig. 3 H). Control experiments on Orai3-WT showed that the initial reduction in current during BMS treatment is caused by reversible block unrelated to reduction of disulfide bonds (Fig. S1). Fig. 3 I summarizes the rates of rise of 2-APB–activated currents for both inward and outward components of the current. We conclude that reduction of a disulfide bridge formed within the Orai3-G158C channel allows 2-APB to enter and activate the channel with kinetics similar to that of Orai3-WT channels. Moreover, because the rapid, exponential rise of current and decrease in reversal potential only occurs subsequent to BMS treatment during 2-APB activation, we conclude that the action of BMS is state dependent; only after 2-APB activation can BMS reduce the disulfide bond.

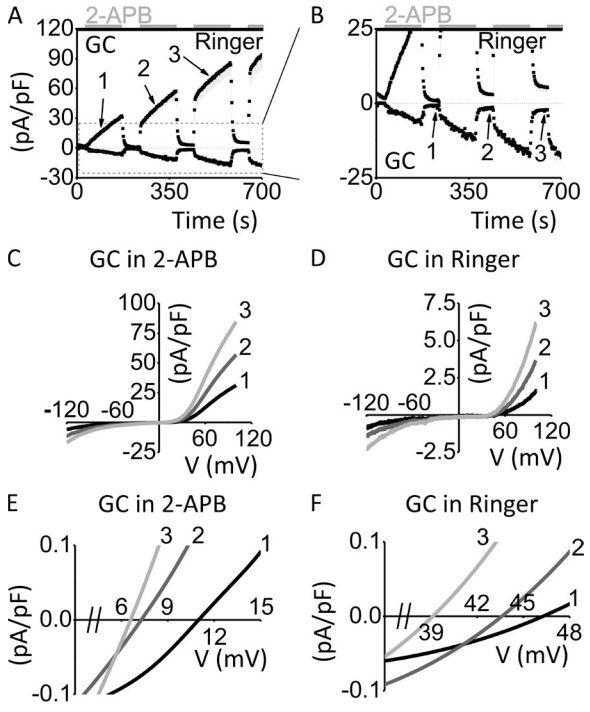

Figure 2. Slow G158C phenotype reveals distinct, 2-APB–induced, open states, characterized by altered reversal potentials. (A and B) Time course of Orai3-G158C (GC), activated by consecutive applications of 100 µM 2-APB for 2 min, interspersed by 1-min-long durations of washout with Ringer solution, represented as mean current density ± SEM (pA/pF) versus time (s; $n = 3$). For clarity, only minus SEM is shown. (C and D) I-V relationships match time points labeled in A and B, respectively. (E and F) Polynomial fits of I-V relationships represented in C and D, respectively, show gradual leftward shift of reversal potential.

Double mutant C101G/G158C abrogates the slow G158C phenotype of 2-APB activation

We next sought to identify the location of the disulfide bridge responsible for the slow phenotype of Orai3-G158C. We reasoned that TM3 position 158 would be buried within the PM and thus would only be able to interact with cysteines that are also positioned within the PM. Of the four endogenous Orai3 cysteines, two are in the extracellular TM3-TM4 loop and two are in TM2. Based on sequence analysis, we hypothesized that C101 of TM2 might be in the vicinity of G158. If this were the case, then C101 might be able to form a disulfide bridge with the introduced cysteine of Orai3-G158C channels, and perhaps in doing so create steric hindrance to 2-APB activation. To test our hypothesis, we generated the double mutant Orai3-C101G/G158C and transfected it into HEK 293A cells. The double mutant behaved much like Orai3-WT; current density rose rapidly, saturated in response to 2-APB application, and declined to zero immediately after 2-APB washout (Fig. 4, A–D). This result is consistent with disulfide bridge formation between TM2 and TM3, which slows the rate of 2-APB channel activation.

Increased 2-APB concentration does not increase the rate of 2-APB activation, instead results in partial block

We also tested whether the slow phenotype exhibited by Orai3-G158C channels might be caused by an altered

dose response of mutant Orai3 channels to 2-APB. To test this, we applied varying concentrations of 2-APB during whole-cell recording. Instead of more rapid activation and increased current density, the higher concentration (1 mM) of 2-APB inhibited further rise or fractionally reduced current density for both Orai3-G158C (Fig. S2, A and B) and Orai3-WT (Fig. S2, C and D). Therefore, the slow activation of Orai3-G158C does not result from a decreased sensitivity to 2-APB.

DISCUSSION

Sequence analysis of Orai channels revealed an internal homology between TM1 and TM3, suggesting evolution of the protein by gene duplication (Cai, 2007). Both TM domains have glutamates toward the extracellular side, glycines at their centers, and an arginine on the intracellular side of TM1 or a tryptophan in TM3. The importance of these TM1 and TM3 residues for ion permeation and gating is reinforced by mutagenesis studies. E106 in Orai1, E81 in Orai3, and E180 in dOrai, each at the extracellular side of TM1, were identified as residues that confer a high degree of Ca^{2+} selectivity (Prakriya et al., 2006; Vig et al., 2006a; Yeromin et al., 2006; Schindl et al., 2008; Demuro et al., 2011). The TM3 glutamates (E190 in Orai1 and E165 in Orai3) also contribute to Ca^{2+} selectivity (Prakriya et al., 2006; Vig et al., 2006a; Yamashita et al., 2007; Schindl et al., 2008). Glycine residues near the middle of TM1 (Zhang et al., 2011) and TM3 (Srikanth et al., 2011) of Orai1 are required for normal STIM-induced gating; a gating hinge mechanisms was proposed. The Orai1 G183A mutation also confers 2-APB sensitivity (Srikanth et al., 2011). Near the intracellular side of TM1, R91 in Orai1 (Feske et al., 2006; Derler et al., 2009; Zhang et al., 2011) and the corresponding R66 in Orai3 (Schindl et al., 2008) are important for channel gating; when mutated to W, the channel is blocked. Moreover, TM3 has a tryptophan residue (W176 in ORAI1 and W151 in Orai3), and the Orai1 W176C mutation results in preactivated channels (Srikanth et al., 2011). Collectively, these studies reinforce functional similarities in TM1 and TM3.

Previous mutagenesis studies and our present results can now be interpreted further in terms of a recently published crystal structure of *Drosophila* Orai (Hou et al., 2012). The crystal structure confirms that each Orai subunit contributes a glutamate residue, positioned atop TM1, to form the selectivity filter. TM1 appears to be bent below the glycine hinge, which is at the center of TM1. The TM1 arginine (lysine in the dOrai structure) assists in anion coordination, which may assist in channel gating by stabilizing the closed state. The crystal structure also validates the notion that TM1 and TM3 are predominantly α-helical and that residues identified by cysteine-scanning mutagenesis (R91, L95, G98, V102, and E106) line the STIM1-activated pore of Orai1 (McNally et al., 2009; Zhou et al., 2010). TM3, however, appears with TM2 as part of a concentric ring that corrals the pore-forming TM1 domains.

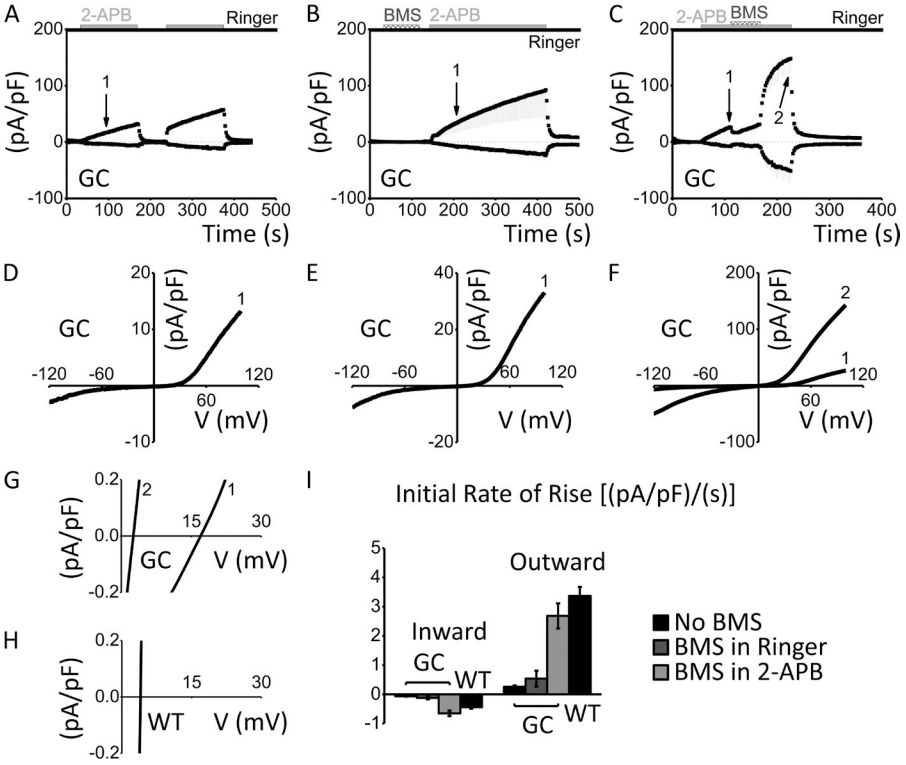

Figure 3. State-dependent reversal of slow G158C phenotype by reducing reagent BMS during 2-APB activation. (A–C) Time courses of Orai3-G158C (GC): no BMS treatment, activated by 100 µM 2-APB ($n = 3$; A), treated with BMS before 2-APB activation ($n = 5$; B), and treated with BMS during 2-APB activation ($n = 3$; C), represented as mean current density ± SEM (pA/pF) versus time (s). For clarity, only minus SEM is shown. (D–F) I-V relationships of Orai3-G158C corresponding to time points (1 min after solution exchange) labeled in time courses A–C, respectively. (G) Polynomial fits of I-V relationships represented in F. (H) Orai3-WT reversal potential (WT trace is zoomed in from Fig. 1 C). (I) Bar graphs summarizing rise of inward and outward components of the 2-APB–activated current density (pA/pF) over time (s; first 30 s after solution exchange) for WT with no BMS treatment (values taken from Fig. 1 I) and for GC, with no BMS treatment, BMS treatment before 2-APB activation, or BMS treatment during 2-APB activation. Error bars show SEM.

In this manuscript, we further probe the Orai3 TM3 central glycine, G158, to understand its role in 2-APB activation. We show that Orai3-G158C channels, but not Orai3-G158A channels, exhibit greatly reduced rates of activation by 2-APB and continued persistent channel activity after 2-APB washout (Fig. 1). Because Orai3-G158A channels do not exhibit altered kinetics of activation, we conclude that mutation G158C does not simply reduce the flexibility of TM3, which might result in this slow phenotype. Moreover, consecutive rounds of 2-APB application/washout reveal two interesting properties of Orai3-G158C channels: (1) reapplication of 2-APB after washout results in current amplitudes similar to those exhibited before washout and (2) just as current densities increase during 2-APB application, amplitudes of residual current after 2-APB exposure progressively increase. Furthermore, reversal potentials of currents carried by Orai3-G158C channels gradually shift leftward, signifying greater pore dilation (Fig. 2 and Fig. S3). Based on these data, we propose that the G158C mutation sterically hinders 2-APB from easily entering and exiting Orai3 channels, thus slowing rates of activation and washout and trapping the channel in distinct open states characterized by altered reversal potentials and extents of pore dilation. The slow G158C phenotype suggests a step-wise mechanism for 2-APB activation in which 2-APB penetrates and activates Orai3 channels by inducing conformational changes leading to distinct intermediate open states, until a complete open state, associated with current density saturation and barely positive reversal potential, is reached.

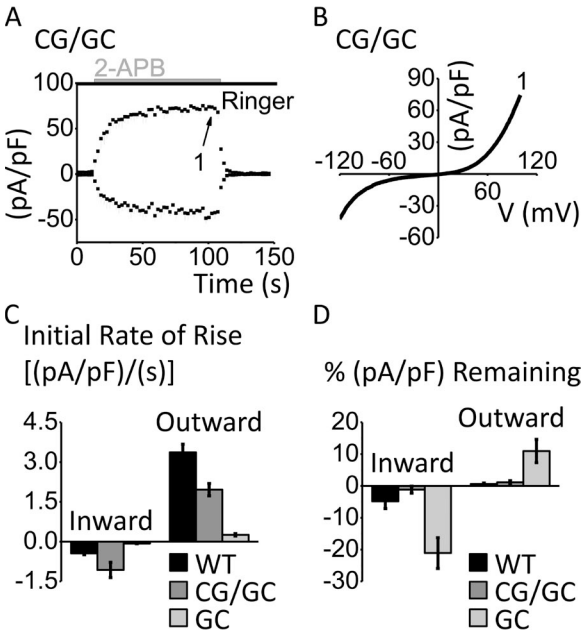

Figure 4. Double mutant Orai3-C101G/G158C abrogates the slow G158C phenotype. (A) Time course of Orai3-C101G/G158C (CG/GC), activated by 100 µM 2-APB (n = 3), represented as mean current density ± SEM (pA/pF) versus time (s). For clarity, only minus SEM is shown. (B) I-V relationship corresponding to labeled time point in A. (C) Bar graph summarizing rise of inward and outward components of the 2-APB–activated current density (pA/pF) over time (s; first 30 s after solution exchange) for Orai3-WT (WT; n = 4), Orai3-C101G/G158C (CG/GC; n = 3), and Orai3-G158C (GC; n = 4). Values for WT and GC are taken from Fig. 1 I. (D) Bar graph summarizing percent current density (pA/pF) remaining 40 s after 2-APB washout compared with current density recorded before 2-APB washout for WT, CG/GC, and GC. Values for WT and GC are taken from Fig. 1 K. Error bars show SEM.

This proposed mechanism of progressive conformational change by pore dilation and decrease in reversal potential during 2-APB activation is similar to the graded mechanism used by STIM molecules, which physically attach to and activate Orai channels (Cahalan, 2009; Soboloff et al., 2012). The physical interaction allows STIM molecules to regulate the CRAC channel's hallmark biophysical properties: Ca^{2+} selectivity (McNally et al., 2012), Ca^{2+}-dependent inactivation (Mullins et al., 2009; Scrimgeour et al., 2009; Hoover and Lewis, 2011), and current amplitude (Scrimgeour et al., 2009; Hoover and Lewis, 2011). Once the optimal ratio of interacting STIM1/Orai1 molecules is reached (2:1), Orai1 channels exhibit maximum Ca^{2+}-dependent inactivation and current density. This concept of graded activation of Orai1 by STIM1 is further supported by a study that used chimeric constructs composed of Orai1 subunits in tandem with the activating, cytosolic regions of STIM1 (Li et al., 2011). The study concluded that current amplitude carried by Orai1 channels increases as more STIM1 molecules bind and that maximum current amplitude is reached when two STIM1 molecules bind to each Orai1 subunit. Although we do not measure the stoichiometry of 2-APB molecules to Orai3-G158C molecules, we do see a trend of greater pore dilation characterized by progressive decrease in reversal potential with increased time of 2-APB treatment, a biophysical hallmark of 2-APB–activated Orai3 (Schindl et al., 2008). Furthermore, 2-APB and STIM1 antagonize each other as modulators of Orai3 channels; STIM1-bound Orai3 channels resist 2-APB activation, whereas 2-APB–activated channels resist STIM1-induced channel opening (Yamashita et al., 2011). We suggest that 2-APB and STIM1 use similar graded mechanisms of activation, both inducing a series of conformational changes upon binding, leading to step-wise opening of the Orai channel. Once the Orai3 channel's conformation changes in response to either 2-APB or STIM1 binding, the channel can no longer accommodate the binding of or interaction with the other modulator. Perhaps as STIM1 binds, the site of 2-APB interaction becomes physically unavailable, and as 2-APB activates the nonselective pore, the sites of STIM1 interaction become physically unavailable.

In this study, we also find that the slow activation by 2-APB exhibited by Orai3-G158C channels can be reversed upon application of reducing reagent BMS, but

in a state-dependent manner, only during channel activation by 2-APB (Fig. 3). This result and the WT behavior of the double mutant Orai3-C101G/G158C (Fig. 4) suggest that a cysteine residue at position 158 forms a disulfide bridge with the endogenous C101 in TM2. This disulfide bridge strains the channel or hinders access and leads to slowed kinetics of 2-APB activation. Furthermore, because the effects of BMS are state dependent, we show that the disulfide bridge formed between G158C and endogenous C101 can only be cleaved when the channel is in its open state. Perhaps as 2-APB dilates the pore, TM1 domains move away from one another, allowing BMS to enter the pore and influence the chemical environment of the nearby TM2/TM3 ring that corrals the TM1 pore–forming segments. We would like to note that even after BMS treatment during 2-APB activation (Fig. 3 C), Orai3-G158C channels exhibited residual current upon 2-APB washout. We propose that this might be caused by (a) incomplete BMS treatment, (b) reformation of disulfide bridges upon BMS washout, or (c) reduced, free cysteines in TM3 of Orai3-G158C preventing complete channel closure. Furthermore, whereas Orai3-C101G/G158C channels exhibit kinetics similar to WT channels, they do carry currents of lower amplitude. We suggest that this is in part caused by overall structural changes that might occur with increased number of mutations within the TM2/TM3 region, which is necessary for Orai3 activation by 2-APB (Zhang et al., 2008). Both double mutants Orai3-C101A/G158C and Orai3-C101S/G158C do not activate upon 2-APB application (Fig. S4), providing further evidence that the 2-APB–binding site is altered.

Finally, with our data and the crystal structure in mind, we suggest that a set of intrasubunit disulfide bridges form between an introduced cysteine at position 158 and the endogenous TM2 C101. The crystal structure demonstrates that TM2 and TM3 domains of Orai subunits are in fact adjacent to each other (Fig. 5, A and B) and that positions C198 and G255 (homologous to C101 and G158 of Orai3) are both pointed toward the center within a single dOrai subunit (Fig. 5 B). The α carbons of these two residues are within 10 Å of one another (Fig. 5, C and D). Perhaps this distance is decreased when the channel is in motion in a physiological setting in real time, or perhaps the G158C mutation itself results in decreased proximity between positions 158 and 101. This work offers the first structural link between the TM2 and TM3 domains of Orai channels, as revealed by site-directed mutagenesis and patch-clamp analysis, and further validates the crystal structure.

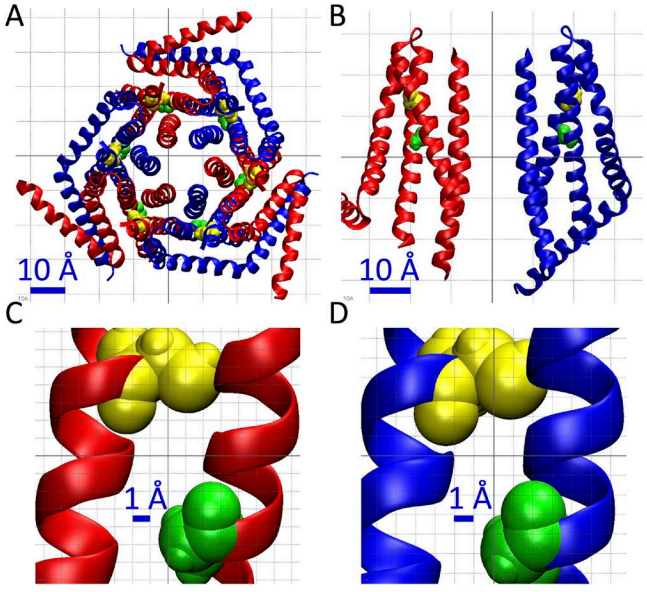

Figure 5. Crystal structure of *Drosophila* Orai (dOrai) predicts locations of Orai3 residues C101 and G158 and proposed intrasubunit disulfide bond. (A and B) Extracellular (A) and side (B; with four of six subunits removed for clarity) views of dOrai. (C and D) Zoomed-in images showing TM2 and TM3 of both subunit types B and A, respectively. Subunit A is depicted as blue α helices, subunit B as red α-helices, C198 (homologous to Orai3 C101) as yellow van der Waals spheres, and G255 (homologous to Orai3 G158) as green van der Waals spheres. α carbons of residues C198 and G255 are within 10 Å of each other.

This work was supported by National Institutes of Health grant NS-14609 (to M.D. Cahalan).

Lawrence G. Palmer served as editor.

Submitted: 15 May 2013
Accepted: 16 August 2013

REFERENCES

Bootman, M.D., P. Lipp, and M.J. Berridge. 2001. The organisation and functions of local Ca^{2+} signals. *J. Cell Sci.* 114:2213–2222.

Cahalan, M.D. 2009. STIMulating store-operated Ca^{2+} entry. *Nat. Cell Biol.* 11:669–677. http://dx.doi.org/10.1038/ncb0609-669

Cai, X. 2007. Molecular evolution and structural analysis of the Ca^{2+} release-activated Ca^{2+} channel subunit, Orai. *J. Mol. Biol.* 368:1284–1291. http://dx.doi.org/10.1016/j.jmb.2007.03.022

DeHaven, W.I., J.T. Smyth, R.R. Boyles, G.S. Bird, and J.W. Putney Jr. 2008. Complex actions of 2-aminoethyldiphenyl borate on store-operated calcium entry. *J. Biol. Chem.* 283:19265–19273. http://dx.doi.org/10.1074/jbc.M801535200

Demuro, A., A. Penna, O. Safrina, A.V. Yeromin, A. Amcheslavsky, M.D. Cahalan, and I. Parker. 2011. Subunit stoichiometry of human Orai1 and Orai3 channels in closed and open states. *Proc. Natl. Acad. Sci. USA.* 108:17832–17837. http://dx.doi.org/10.1073/pnas.1114814108

Derler, I., M. Fahrner, O. Carugo, M. Muik, J. Bergsmann, R. Schindl, I. Frischauf, S. Eshaghi, and C. Romanin. 2009. Increased hydrophobicity at the N terminus/membrane interface impairs gating of the severe combined immunodeficiency-related ORAI1 mutant. *J. Biol. Chem.* 284:15903–15915. http://dx.doi.org/10.1074/jbc.M808312200

Feske, S., Y. Gwack, M. Prakriya, S. Srikanth, S.H. Puppel, B. Tanasa, P.G. Hogan, R.S. Lewis, M. Daly, and A. Rao. 2006. A mutation in Orai1 causes immune deficiency by abrogating CRAC channel function. *Nature.* 441:179–185. http://dx.doi.org/10.1038/nature04702

Hoover, P.J., and R.S. Lewis. 2011. Stoichiometric requirements for trapping and gating of Ca^{2+} release-activated Ca^{2+} (CRAC)

channels by stromal interaction molecule 1 (STIM1). *Proc. Natl. Acad. Sci. USA.* 108:13299–13304. http://dx.doi.org/10.1073/pnas.1101664108

Hou, X., L. Pedi, M.M. Diver, and S.B. Long. 2012. Crystal structure of the calcium release-activated calcium channel Orai. *Science.* 338:1308–1313. http://dx.doi.org/10.1126/science.1228757

Li, Z., L. Liu, Y. Deng, W. Ji, W. Du, P. Xu, L. Chen, and T. Xu. 2011. Graded activation of CRAC channel by binding of different numbers of STIM1 to Orai1 subunits. *Cell Res.* 21:305–315. http://dx.doi.org/10.1038/cr.2010.131

Liou, J., M.L. Kim, W.D. Heo, J.T. Jones, J.W. Myers, J.E. Ferrell Jr., and T. Meyer. 2005. STIM is a Ca^{2+} sensor essential for Ca^{2+}-store-depletion-triggered Ca^{2+} influx. *Curr. Biol.* 15:1235–1241. http://dx.doi.org/10.1016/j.cub.2005.05.055

Lis, A., C. Peinelt, A. Beck, S. Parvez, M. Monteilh-Zoller, A. Fleig, and R. Penner. 2007. CRACM1, CRACM2, and CRACM3 are store-operated Ca^{2+} channels with distinct functional properties. *Curr. Biol.* 17:794–800. http://dx.doi.org/10.1016/j.cub.2007.03.065

McNally, B.A., M. Yamashita, A. Engh, and M. Prakriya. 2009. Structural determinants of ion permeation in CRAC channels. *Proc. Natl. Acad. Sci. USA.* 106:22516–22521. http://dx.doi.org/10.1073/pnas.0909574106

McNally, B.A., A. Somasundaram, M. Yamashita, and M. Prakriya. 2012. Gated regulation of CRAC channel ion selectivity by STIM1. *Nature.* 482:241–245.

Mullins, F.M., C.Y. Park, R.E. Dolmetsch, and R.S. Lewis. 2009. STIM1 and calmodulin interact with Orai1 to induce Ca^{2+}-dependent inactivation of CRAC channels. *Proc. Natl. Acad. Sci. USA.* 106:15495–15500. http://dx.doi.org/10.1073/pnas.0906781106

Parekh, A.B., and J.W. Putney Jr. 2005. Store-operated calcium channels. *Physiol. Rev.* 85:757–810. http://dx.doi.org/10.1152/physrev.00057.2003

Peinelt, C., A. Lis, A. Beck, A. Fleig, and R. Penner. 2008. 2-Aminoethoxydiphenyl borate directly facilitates and indirectly inhibits STIM1-dependent gating of CRAC channels. *J. Physiol.* 586:3061–3073. http://dx.doi.org/10.1113/jphysiol.2008.151365

Prakriya, M., S. Feske, Y. Gwack, S. Srikanth, A. Rao, and P.G. Hogan. 2006. Orai1 is an essential pore subunit of the CRAC channel. *Nature.* 443:230–233. http://dx.doi.org/10.1038/nature05122

Putney, J.W. Jr. 1986. A model for receptor-regulated calcium entry. *Cell Calcium.* 7:1–12. http://dx.doi.org/10.1016/0143-4160(86)90026-6

Roos, J., P.J. DiGregorio, A.V. Yeromin, K. Ohlsen, M. Lioudyno, S. Zhang, O. Safrina, J.A. Kozak, S.L. Wagner, M.D. Cahalan, et al. 2005. STIM1, an essential and conserved component of store-operated Ca^{2+} channel function. *J. Cell Biol.* 169:435–445. http://dx.doi.org/10.1083/jcb.200502019

Schindl, R., J. Bergsmann, I. Frischauf, I. Derler, M. Fahrner, M. Muik, R. Fritsch, K. Groschner, and C. Romanin. 2008. 2-aminoethoxydiphenyl borate alters selectivity of Orai3 channels by increasing their pore size. *J. Biol. Chem.* 283:20261–20267. http://dx.doi.org/10.1074/jbc.M803101200

Scrimgeour, N., T. Litjens, L. Ma, G.J. Barritt, and G.Y. Rychkov. 2009. Properties of Orai1 mediated store-operated current depend on the expression levels of STIM1 and Orai1 proteins. *J. Physiol.* 587:2903–2918. http://dx.doi.org/10.1113/jphysiol.2009.170662

Soboloff, J., B.S. Rothberg, M. Madesh, and D.L. Gill. 2012. STIM proteins: dynamic calcium signal transducers. *Nat. Rev. Mol. Cell Biol.* 13:549–565. http://dx.doi.org/10.1038/nrm3414

Srikanth, S., M.K. Yee, Y. Gwack, and B. Ribalet. 2011. The third transmembrane segment of orai1 protein modulates Ca^{2+} release-activated Ca^{2+} (CRAC) channel gating and permeation properties. *J. Biol. Chem.* 286:35318–35328. http://dx.doi.org/10.1074/jbc.M111.265884

Vig, M., A. Beck, J.M. Billingsley, A. Lis, S. Parvez, C. Peinelt, D.L. Koomoa, J. Soboloff, D.L. Gill, A. Fleig, et al. 2006a. CRACM1 multimers form the ion-selective pore of the CRAC channel. *Curr. Biol.* 16:2073–2079. http://dx.doi.org/10.1016/j.cub.2006.08.085

Vig, M., C. Peinelt, A. Beck, D.L. Koomoa, D. Rabah, M. Koblan-Huberson, S. Kraft, H. Turner, A. Fleig, R. Penner, and J.P. Kinet. 2006b. CRACM1 is a plasma membrane protein essential for store-operated Ca^{2+} entry. *Science.* 312:1220–1223. http://dx.doi.org/10.1126/science.1127883

Yamashita, M., L. Navarro-Borelly, B.A. McNally, and M. Prakriya. 2007. Orai1 mutations alter ion permeation and Ca^{2+}-dependent fast inactivation of CRAC channels: Evidence for coupling of permeation and gating. *J. Gen. Physiol.* 130:525–540. http://dx.doi.org/10.1085/jgp.200709872

Yamashita, M., A. Somasundaram, and M. Prakriya. 2011. Competitive modulation of Ca^{2+} release-activated Ca^{2+} channel gating by STIM1 and 2-aminoethyldiphenyl borate. *J. Biol. Chem.* 286:9429–9442. http://dx.doi.org/10.1074/jbc.M110.189035

Yeromin, A.V., S.L. Zhang, W. Jiang, Y. Yu, O. Safrina, and M.D. Cahalan. 2006. Molecular identification of the CRAC channel by altered ion selectivity in a mutant of Orai. *Nature.* 443:226–229. http://dx.doi.org/10.1038/nature05108

Zhang, S.L., Y. Yu, J. Roos, J.A. Kozak, T.J. Deerinck, M.H. Ellisman, K.A. Stauderman, and M.D. Cahalan. 2005. STIM1 is a Ca^{2+} sensor that activates CRAC channels and migrates from the Ca^{2+} store to the plasma membrane. *Nature.* 437:902–905. http://dx.doi.org/10.1038/nature04147

Zhang, S.L., J.A. Kozak, W. Jiang, A.V. Yeromin, J. Chen, Y. Yu, A. Penna, W. Shen, V. Chi, and M.D. Cahalan. 2008. Store-dependent and -independent modes regulating Ca^{2+} release-activated Ca^{2+} channel activity of human Orai1 and Orai3. *J. Biol. Chem.* 283:17662–17671. http://dx.doi.org/10.1074/jbc.M801536200

Zhang, S.L., A.V. Yeromin, J. Hu, A. Amcheslavsky, H. Zheng, and M.D. Cahalan. 2011. Mutations in Orai1 transmembrane segment 1 cause STIM1-independent activation of Orai1 channels at glycine 98 and channel closure at arginine 91. *Proc. Natl. Acad. Sci. USA.* 108:17838–17843. http://dx.doi.org/10.1073/pnas.1114821108

Zhou, Y., S. Ramachandran, M. Oh-Hora, A. Rao, and P.G. Hogan. 2010. Pore architecture of the ORAI1 store-operated calcium channel. *Proc. Natl. Acad. Sci. USA.* 107:4896–4901. http://dx.doi.org/10.1073/pnas.1001169107